23

Fabrication and Characterizations of Multi-Layer Thin Film Internal Antenna for Wireless Communication

Book-Sung Park, Hyun-Sang Lee and Soren Pedersen
Nokia, MS Symbian Smartphones Device R&D
Republic of Korea
United States of America
Denmark

1. Introduction

In 1990s, mobile communications were developed based on the Code Division Multiple Access (CDMA) which is used in Korea, USA, and Japan and Global System for Mobile communications (GSM) which is used in Europe and other countries. Beginning in 2000s, global roaming was required for unifying these two communication methods, but the different frequency allocations in various countries impeded the unification. Therefore, the complexities of mobile handsets were increased to support 2G, 2.5G, and 3G at the same time. The development of semiconductor technique makes it necessary to upgrade the electronic components which are smaller and more powerful than those used in the multimedia and frequency bands of the early 1990s(F. Adachi et al., 1998). This kind of growth of electronic components means that handsets have more complex functions and a reduced size. And the antenna which is used for the mobile communicating set has been changed from an external one to an internal one thing. The internal antenna allows the handset to be small and easily portable (K. Hirasawa & M. Haneishi, 1991). For that reason, most of handset has the internal antenna these days. The internal antennas of several kinds of design techniques such as monopole antenna, Planar Inverted-F Antenna (PIFA) antenna, and high dielectric internal antenna are used and studied in many companies and research labs (W. L. Stutzman & G. A. Thiele, 1998). The monopole antenna has one feeding point basis on dipole antenna topology and the advantage is small size and wide frequency bandwidth on the other hand the disadvantage is that its radiation characteristic is more affected by its surroundings such as ground, user's body, hand, and head than the others. The PIFA has both of the feeding and shorting point and the advantage is that the radiation performance cannot be affected by human and ground condition, impedance matching and the Total Radiated Power (TRP), Total Isotropic Sensitivity (TIS) and Special Absorption Rate (SAR) performance is better than that of monopole antenna, but the frequency bandwidth is narrower than monopole antenna. The high dielectric antenna is consisted of high dielectric materials and metal antenna patterns. This technique is the best solution pertaining to the size, but the cost is the worst. So, the PIFA type internal antenna is the most interested solution and is studied in labs and companies.

The proposed sputter-deposited multilayer thin film internal antenna solution is a technological revolution. Thus, the sputter-deposited multilayer thin film internal antenna solution is better off compare with the current carrier-based internal antenna method. This new manufacturing technology on internal antenna can achieve the advanced antenna development. For realization of this method, antenna meander pattern is sputtered on the cover of handset material which is polycarbonate substrate by DC sputter-deposited method(D. Yuepeng, 2005). Especially, the sputter-deposited internal antenna performance is better than the ink print method antenna that was recently proposed. Because the ink print method is can't get a good uniformity of antenna meander line with the ink print method. For this reason, ink print method cannot get the uniformity of molecule density and this will make some degradation on the antenna performance. Owing to the sputter-deposited internal antenna method on polycarbonate is vastly attractive to the next generation 4G Multiple-Input Multiple-Output (MIMO) system.

2. Experiment results and discuss of the multilayer thin film

2.1 Multilayer thin film fabrication

The multilayer thin film internal antenna solutions are presented based on the precursor with the Ni/Ag thin film solution. The overall size is 43.0 × 24.0 × 0.0015mm^3 (height: 1.5um). Figure 1 illustrates a flow diagram of fabrication processes with the Ni/Ag/Ni thin film. The sputtering parameters and co-sputtering techniques of the experiments are listed in Table 1(G. C. Stutzin et al., 1993). This section describes co-techniques and fabrication processes.

To begin with, the proposed multilayer thin films fabricate of the tri-structural layer with the Ni and Ag material. Actually, the multilayer thin film solution needs a previous work, spray-coating with 80um spray-coating process on the polycarbonate substrate at 80°C for 90 minutes used WP100 material. This is the reason why the polycarbonate surface is seriously rough to be adapted to wireless mobile propagation application. Therefore, the multilayer (Ni/Ag/Ni) thin film radiators need for the compensate material as well as WP100 materials can compensate for surface flatness.

Second, the multilayer internal antenna is composed of three stacked layer(Ni/Ag/Ni). The first layer is called the adhesion layer, the adhesion layer is made by growth of Ni material with 3,000Å thickness on poly carbonate substrate and the sputtering condition was 7 KW per 180 seconds in plasma circumstances. The second layer is defined as the conducted layer, conducted layer is manufactured by growth of Ag material on the Ni layer, total experimental sputtering thickness is approximately 8,000Åwith 7 KW per 1,500 seconds conditions. And the last layer is defined as the safeguard layer, safeguard layer is manufactured by growth of Ni material with 4,000Å thickness with 7 KW per 240 seconds conditions.

Last, the multilayer thin film radiator is characterized by Energy-dispersive X-ray spectroscopy (EDX) and analysis of cross-sectional structures is observed by field-emission scanning electron microscopy (FE-SEM). The standing wave ratio characteristic is measured with Agilent E5071B Network Analyzer and Agilent ADS simulation system was used for getting the optimum standing wave ratio. The quad-band TRP and TIS characteristics are measured in an anechoic chamber with CTIA (CTIA Certification, 2005).

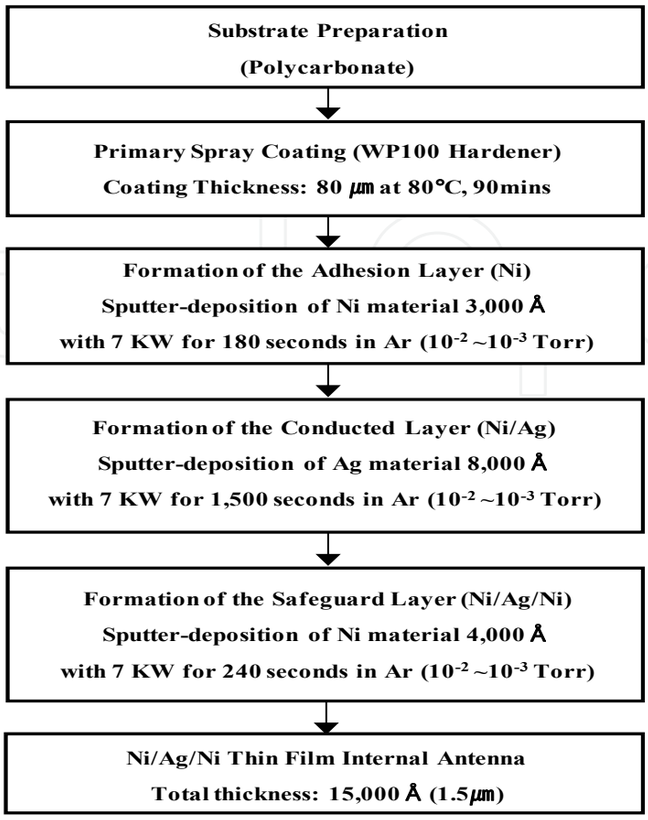

Fig. 1. Fabrication flow for multilayer (Ni/Ag/Ni) thin film process solution; Total thickness target 15,000Å (1.5um)

Target material	Power	Ar flow	Distance (target to substrate)	Time
Ni	7 KW	70 sccm	70mm	180 s
Ag	7 KW	70 sccm	70mm	1500 s
Ni	7 KW	70 sccm	70mm	240 s

Table 1. Experiments sputtering parameters and co-sputtering technique (Ni/Ag/Ni thin film)

2.2 Geometry of the multilayer thin film internal antenna

The configurations of quad-band planar inverted-F antennas have either modified L-shaped slots on the radiating patch in Figure 2. The geometry of quad-band PIFA antenna is shown in Figure 2 (C. T. P. Song et al., 2000).

Figure 2 (a) shows geometry configuration with PCB (RCC ε_r = 3.40, CCL ε_r = 4.20 at under 3GHz) and rear side view of sputter-deposit internal antenna in Figure 2 (b), and Figure 2 (c) is front side view of sputter-deposit internal antenna. To understand the operation of our design with a conventional PIFA using air dielectric with dimensions (l, w) = (43.0, 24.0)mm,

height h = 0.0015mm in which the shorting and feeding are located at center of the plate as shown in Figure 2 (b).

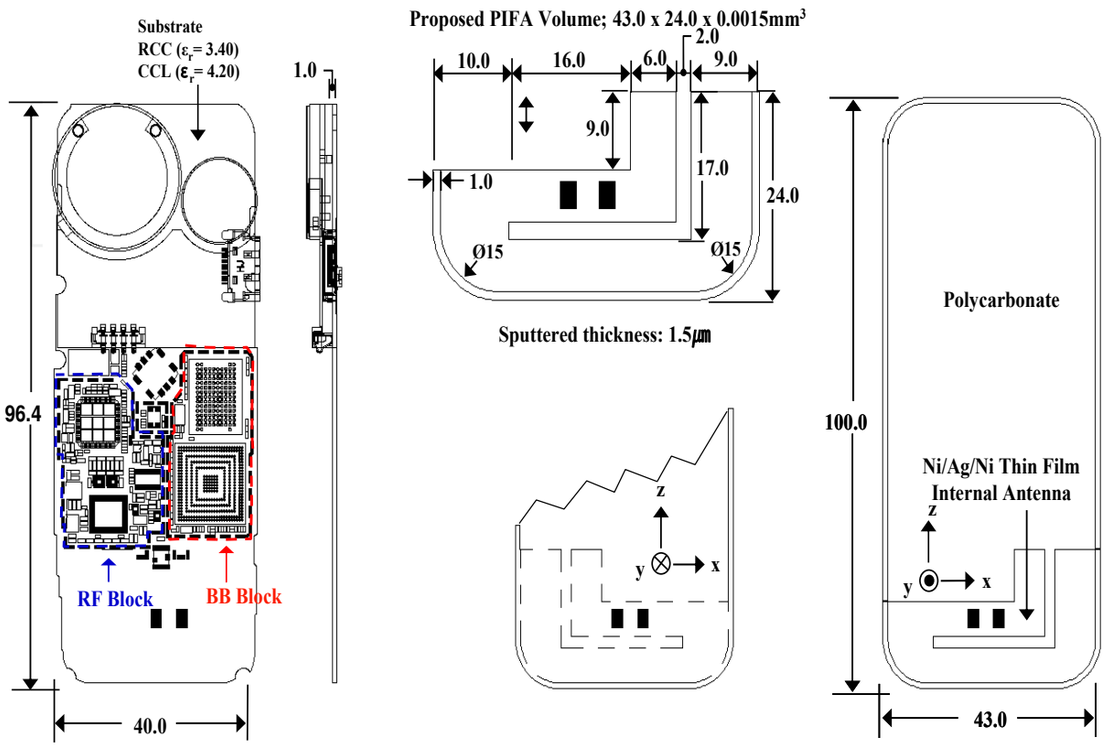

Fig. 2. Geometry configuration of the multilayer thin film internal antenna by sputter-deposited; (a) Geometry configuration of the PCB and quad-band part placement, (b) Rear side view of the sputter-deposit planar inverted-F antenna, (c) Front side view of the sputter-deposit planar inverted-F antenna

2.3 Fabrication of the Ni/Ag/Ni thin film internal antenna

Figure 3 shows an investigated scheme for the Ni/Ag/Ni thin film based on Ni layer. The sputter-deposit Ni/Ag/Ni thin film radiators are composed of primary incident ions, reflect ions, secondary electrons and sputtered atoms on polycarbonate substrate with Ar^+ ion in plasma circumstances. Currently, there are many materials that are characterized for frequency versus skin depth effect. Along with the analysis data, the sputtered thickness should be decreased as the frequency goes high. Figure 4 shows estimated sputtering target thickness on frequency plane. The experimental total target thickness is 1.5um. As the experimental results, the Ni material has best performance in the skin depth aspect. However, characteristics of the Ni resistivity is poor than Ag or Cu materials. I got results of the novel typed Ni/Ag/Ni thin film through many times of trial and error, also in this research suggested the best way to solve the problem. The proposed Ni/Ag/Ni thin film combinations are composed of three stack layer. Figure 4 shows the experiment condition of target thickness and frequency range for Ni/Ag/Ni thin film. The growth of Ni/Ag/Ni thin films are each 3.0×10^3Å, 8.0×10^3Å and 4.0×10^3Å.

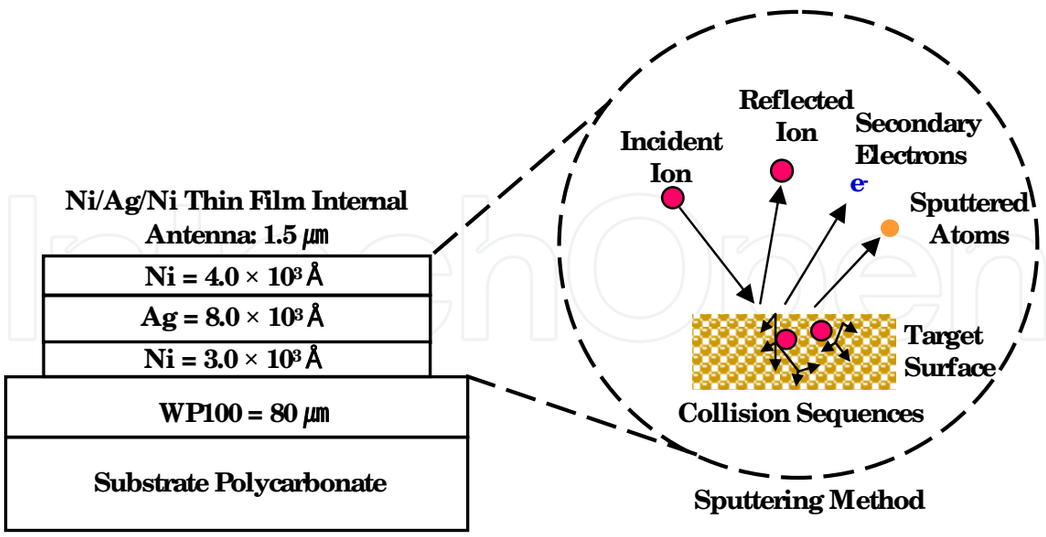

Fig. 3. Cross-section of the experimental procedure for the Ni/Ag/Ni thin film

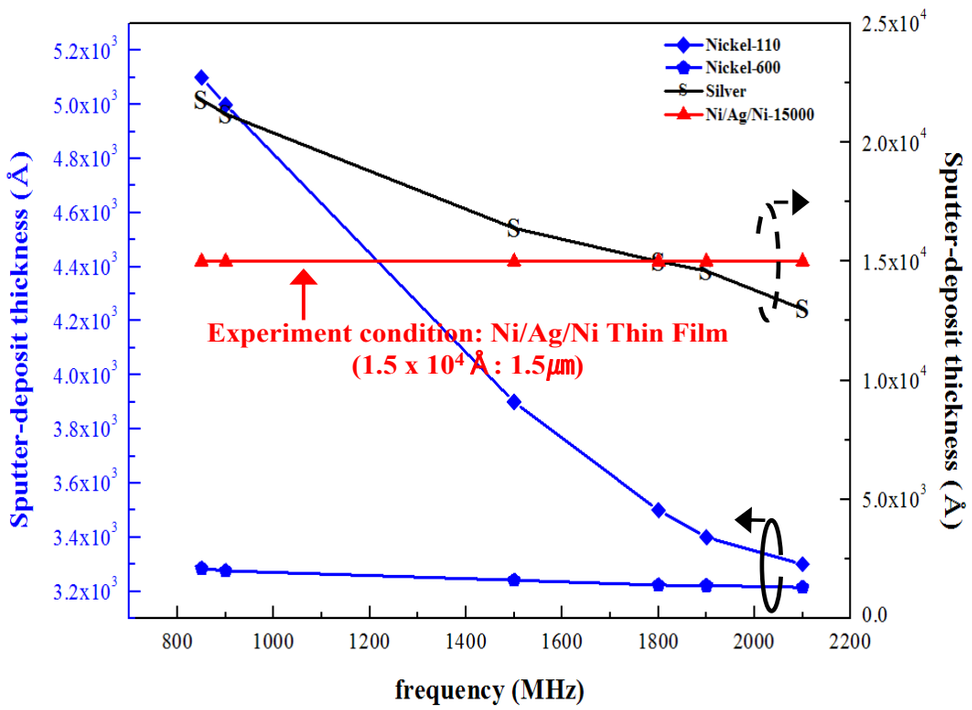

Fig. 4. Experiment conditions of target thickness and frequency range (Ni/Ag/Ni)

Figure 5 shows fabrication process of three stacked Ni/Ag/Ni thin film radiator. This research studied the Ni/Ag/Ni thin film radiator with growth of Ni and Ag. The estimated and measured total radiator thickness is 1.5um. Measurement of the adhesion layer thickness is 3.0 × 10³Å by growth of Ni material on poly carbonate substrate. The Sputter-deposition condition is 7 KW per 180 seconds in plasma circumstances. And then, the

measurement of the conducted layer thickness is 8.0 × 10^3Å by the growth of Ag material on the adhesive layer. The Sputter-deposition condition is 7 KW per 1,500seconds. The last measurement of safeguard layer thickness is 4.0 × 10^3Å by Ni material on Ni/Ag stack layer with thickness with 7 KW per 240 seconds.

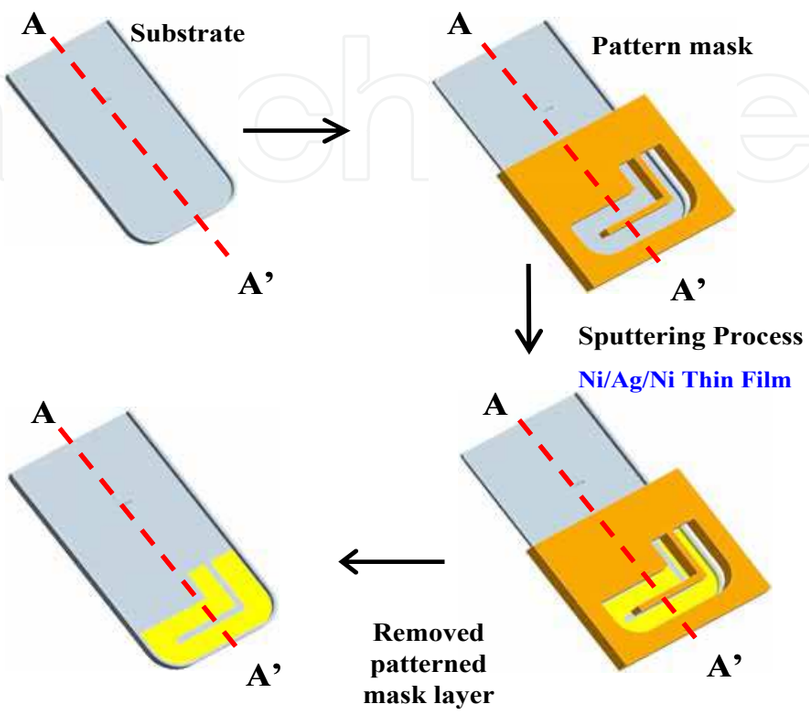

Fig. 5. Fabrication processes of the Ni/Ag/Ni thin film radiator on polycarbonate substrate

Figure 6 shows the pilot sample photo image of the Ni/Ag/Ni thin film, the measurement of the total cavity of sputter-deposited antenna is 43.0 × 24.0 × 0.0015mm^3(sputter-deposit thickness: 1.5um). This work has an enormous benefit for the height between ground plane and antenna height. The actual measured height is 9.5mm from PCB ground to Ni/Ag/Ni thin film internal antenna. Also, this research used contact feeding method for mobile application. Figure 6 shows photo image and geometry information for the Ni/Ag/Ni thin film radiator having resonant frequencies available for quad-band. The electrical length of each associated radiating element closely corresponds to each quarter-wavelength ($\lambda_g/4$) from the feed point A to B and C and D. Next, this research designed radiator pattern for GSM 850 and E-GSM band from A to B also estimated the GSM 1800/GSM 1900 band radiated pattern from C to D at 1710 MHz to 1990 MHz. Actually, A to B meander pattern and C to D meander pattern are significant to characterized of S_{11} and SWR also width and gap distance are key element. Figure 7 shows SEM images of the sputter-deposited Ni/Ag/Ni thin film. It shows surface is uniform magnifying view. Figure 7 (a) shows primary growth image of Ni surface with × 25,000, 30.0kV and 6.0um conditions, Figure 7 (b) shows redundancy layer image for Ag surface (× 10,000, 30.0kV and 8.8um), Figure 7 SEM photo image shows last layer for Ni surface (× 1,000, 30.0kV and 8.8um), and Figure 7 (d) shows interfacial tension image of the sputter-deposit Ni/Ag/Ni thin film. The total thickness of Ni/Ag/Ni thin film seemed to be 100um.

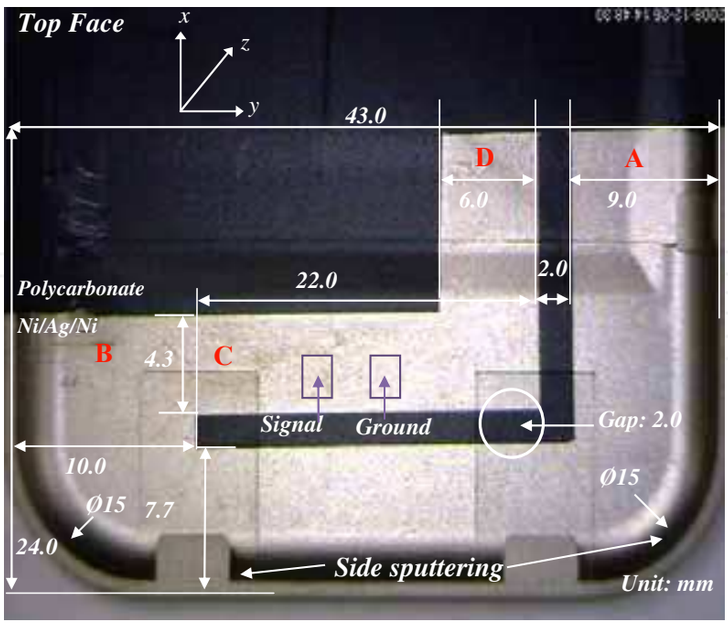

Fig. 6. Prototype photo image of the Ni/Ag/Ni thin film internal antenna by sputter – deposited

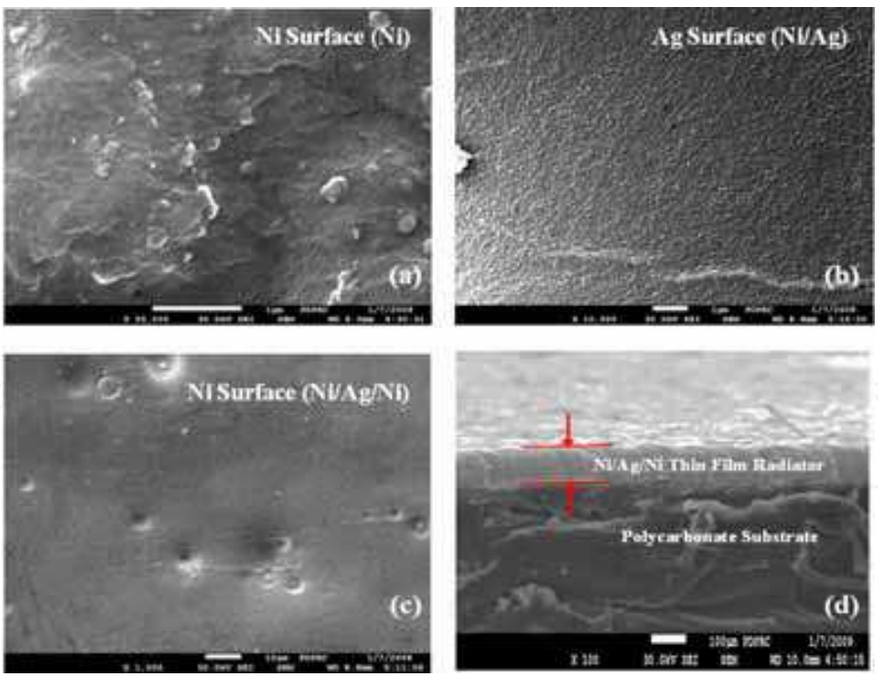

Fig. 7. SEM images of the Ni/Ag/Ni thin films by sputter-deposited. (a) primary growth image of the Ni surface with × 25,000, 30.0kV and 6.0um, (b) redundancy growth image of the Ag surface with × 10,000, 30.0kV and 8.8um, (c) last growth image of the Ni surface with × 1,000, 30.0kV and 8.8um, (d) Interfacial tension image of the Ni/Ag/Ni thin film by sputter-deposited

Figure 8 shows of the material spectrums distribution image for the Ni/Ag/Ni thin film radiator. Figure 8 (a) shows the properties of materials distribution result at Ni surface layer from 0keV to 12keV, the Ni material spread distributions are each 0.743 keV, 0.762 keV, 0.851 keV, 7.478 keV, and 8.265 keV. Figure 8 (b) shows of the Ag material distribution properties curve on Ni material surface also the Ag material spread distributions are each 2.643 keV, 2.806 keV, 2.984 keV, and 3.151 keV. The Ni material characteristic of peak-to-peak is 0.743 keV and the Ag material peak-to-peak is 2.634 keV. Figure 8 (c) shows of the Ni surface (Ni/Ag/Ni) spectra image and of material properties spread spectrum for both materials (Ag and Ni).

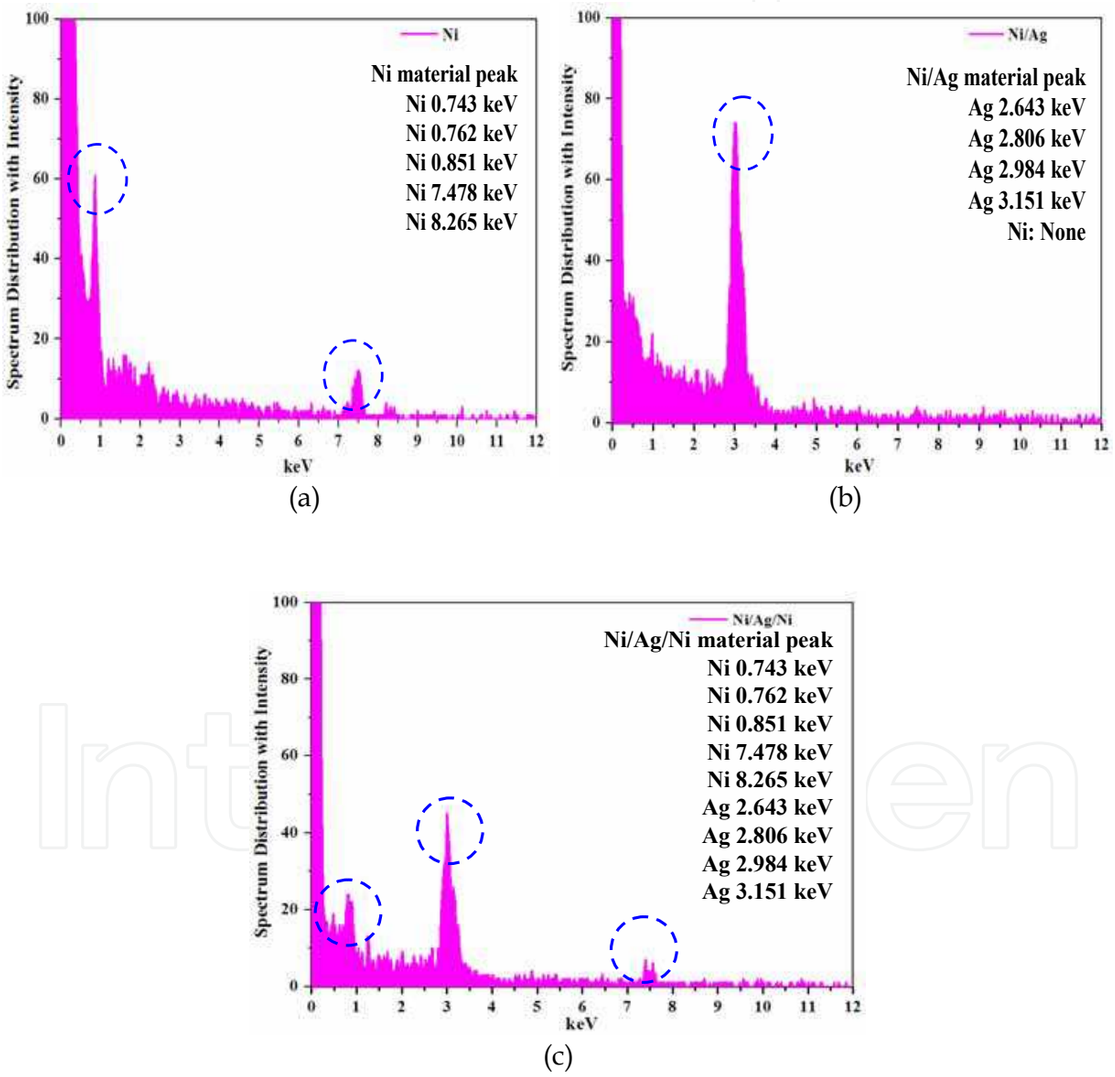

Fig. 8. The Energy-dispersive X-ray spectroscopy pattern images for Ni surface and Ag surface on Ni/Ag/Ni thin film. (a) Spectra image of Ni surface, (b) spectra image of Ni/Ag, (c) spectra image of Ni/Ag/Ni surface

2.4 Characteristics of SWR for the Ni/Ag/Ni thin film internal antenna by sputter-deposited

Figure 9 shows the measurement results of the SWR for prototyped sputter-deposit internal antenna versus optimized with the Ni/Ag/Ni thin film. The operated frequency range is 800 MHz to 2.0 GHz measurement used by Agilent Network Analyzer (E5071B). Figure 9 shows SWR characteristics of the prototyped Ni/Ag/Ni thin film internal antenna and optimized one. The SWR results of prototyped one are indicates each 3.13, 3.17, 3.09 and 2.22 at 824 MHz, 960 MHz, 1710 MHz and 1990 MHz. On the contrary, the case of the optimized Ni/Ag/Ni thin film radiator's SWRs are each 2.18, 2.52, 3.55, and 2.27 at 824 MHz, 960 MHz, 1710 MHz and 1990 MHz, respectively which is fine-tuned with phi type matching network through Agilent ADS simulation. Figure 10 shows of the prototyped Ni/Ag/Ni thin film internal antenna and optimized Ni/Ag/Ni thin film internal antennas S_{11} characteristics. In Figure 10 show prototyped thin film S_{11} result. The measured of S_{11} are each -5.74 dB and -5.67 dB at 824 MHz and 960 MHz also -5.82 dB and -8.44 dB at 1710 MHz to 1990 MHz. On the contrary, optimized internal antenna results marks -8.60 dB, -7.26 dB, -5.01 dB, and -8.22 dB at 824 MHz, 960 MHz, 1710 MHz and 1990 MHz, respectively.

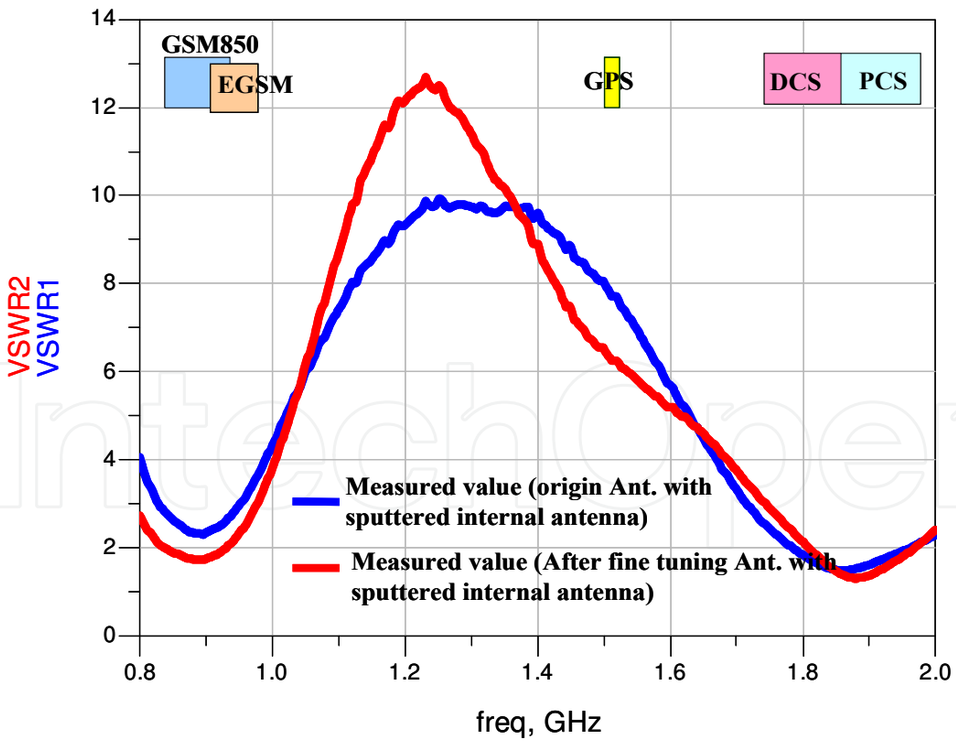

Fig. 9. Measured SWR result comparison the sputter-deposit internal antenna versus after fine tuning the Ni/Ag/Ni thin film internal antenna

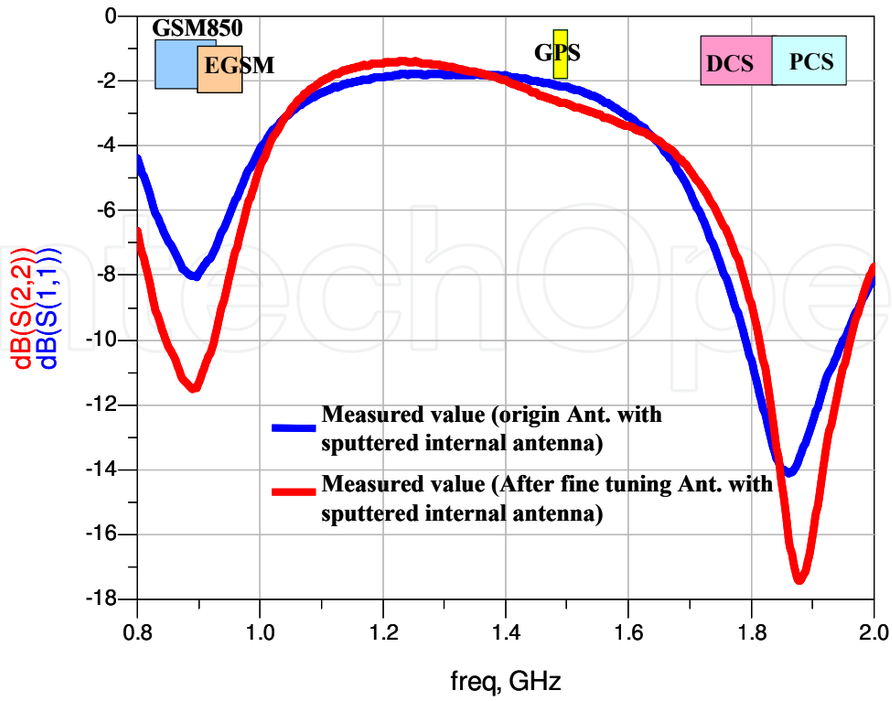

Fig. 10. Measured S_{11} result comparison the sputter-deposit internal antenna versus after fine tuning the Ni/Ag/Ni thin film internal antenna

2.5 Characteristics of current distribution for the Ni/Ag/Ni thin film internal antenna by sputter-deposited

In this experiment describes effect of current distribution for the Ni/Ag/Ni thin film internal antenna. The Ni/Ag/Ni thin film internal antenna solution is efficient rate in each frequency ranges. The prototyped Ni/Ag/Ni thin film internal antenna's overall size is 43.0 × 24.0 × 0.0015mm^3. The simulation result shows 131A/m and 44.5A/m at 870MHz and 1990MHz. Figure 11 and Figure 12 shows the optimized current distribution results for the Ni/Ag/Ni sputter-deposit internal antenna. The measured current distribution ratio of optimized Ni/Ag/Ni sputter-deposit internal antenna is better off than prototype internal antenna. Figure 13 and Figure 14 shows efficiency distribution image for the optimized Ni/Ag/Ni sputter-deposit internal antenna at 870MHz and 1990MHz, total efficiency result are 47% and 55% in par field condition, respectively.

Figure 15 through Figure 18 shows of the 3D far-field (theta and phi) simulated radiation pattern results for the optimized sputter-deposit internal antenna in free space and SAM condition. The simulated frequency range is 870MHz and 1990MHz used by SEMCAD computing program. The results of measured 3D far-field TRP and TIS shows good performance in free space and SAM condition also measured directivity and gains as well as total efficiency rate are agreed well at 870MHz to 1990MHz. The measured of TRP simulation results are each 28.84dBm and 28.30dBm at 870MHz and 1990MHz with SAM condition. Also, measured of TIS simulation results are -101.85dBm and -101.31dBm at 870MHz and 1990MHz with SAM condition. The simulated results listed in Table 2 at free space and SAM condition. The measured two kinds of the experiment is significant meaning which is consumer related aspect.

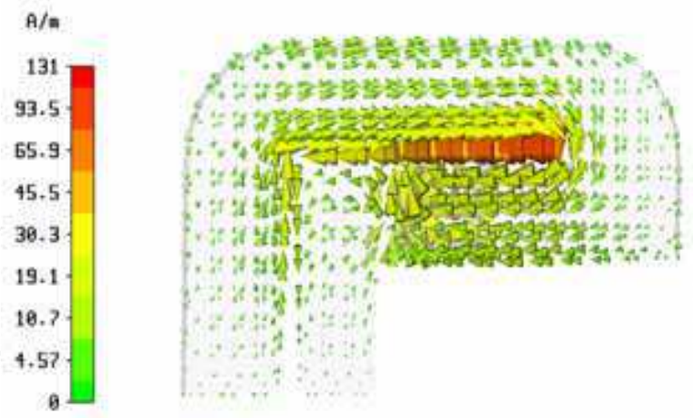

Fig. 11. Optimized current distribution image of the pilot radiator with Ni/Ag/Ni thin film internal antenna handset at 870MHz with CST program (Computer Simulation Technology)

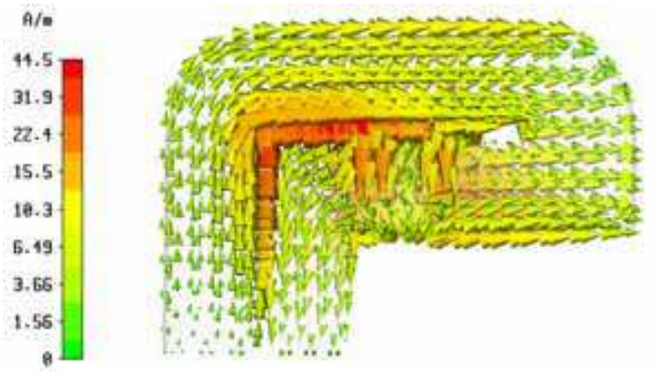

Fig. 12. Optimized current distribution image of the pilot radiator with Ni/Ag/Ni thin film internal antenna handset at 1990MHz with CST program

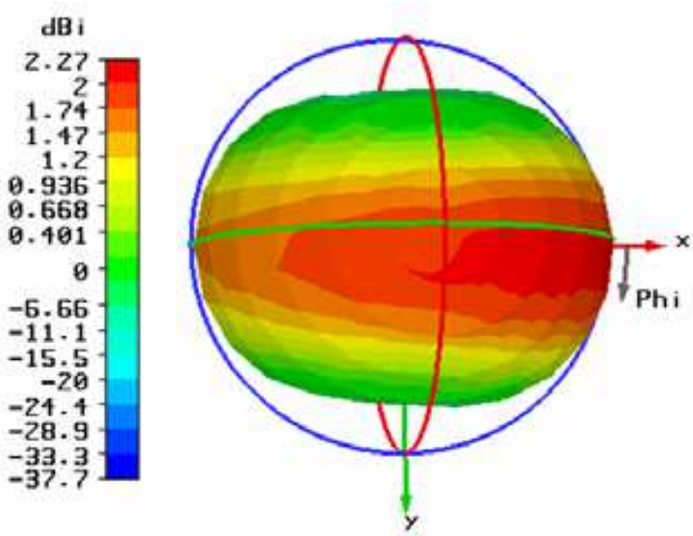

Fig. 13. Optimized total power distribute efficiency image of the pilot radiator with Ni/Ag/Ni thin film internal antenna handset at 870MHz (with CST program)

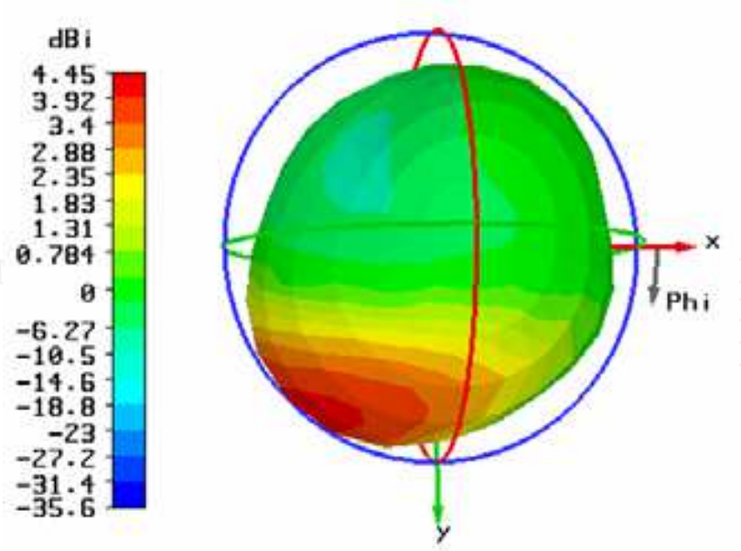

Fig. 14. Optimized total power distribute efficiency image of the pilot radiator with Ni/Ag/Ni thin film internal antenna handset at 1990MHz (with CST program)

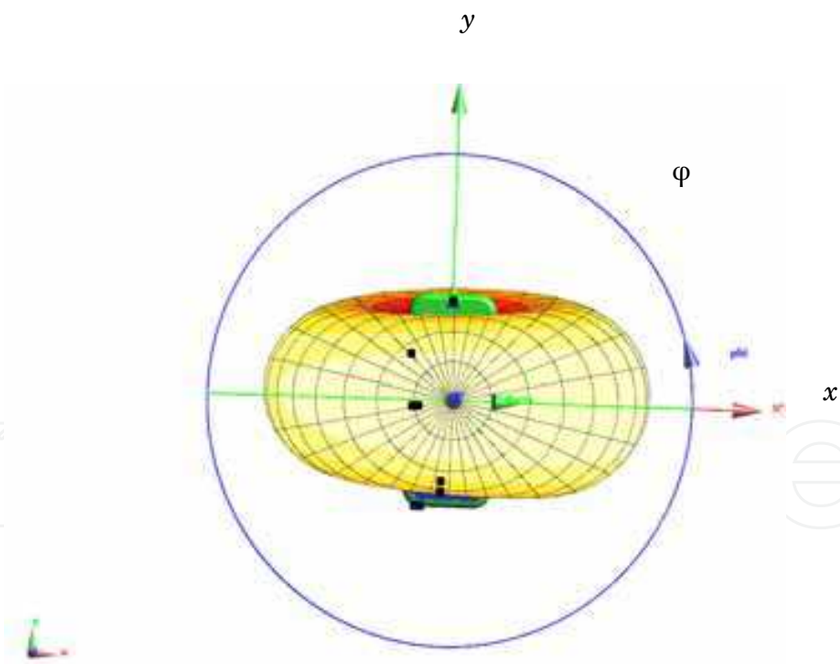

Fig. 15. Optimized 3D Far-field (θ , φ) radiation pattern image of the pilot radiator with Ni/Ag/Ni thin film internal antenna handset at 870MHz free space condition (with SEMCAD program)

Obviously say, the simulated and measured results of the proposed Ni/Ag/Ni sputter-deposit internal antenna show good agreement with each other in free space and SAM condition.

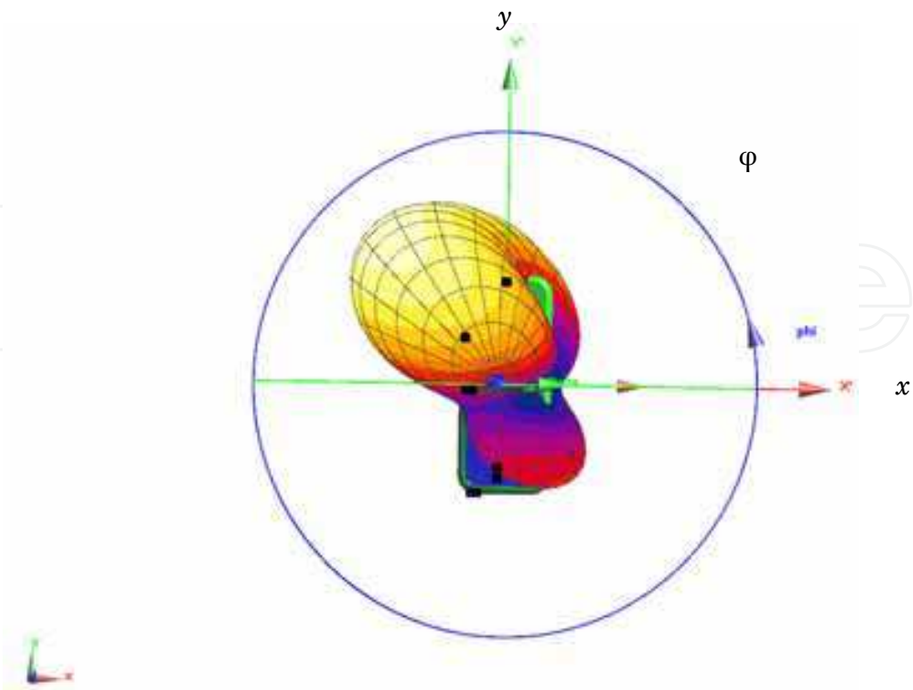

Fig. 16. Optimized 3D Far-field (θ , φ) radiation pattern image of the pilot radiator with Ni/Ag/Ni thin film internal antenna handset at 1990MHz free space condition (with SEMCAD program)

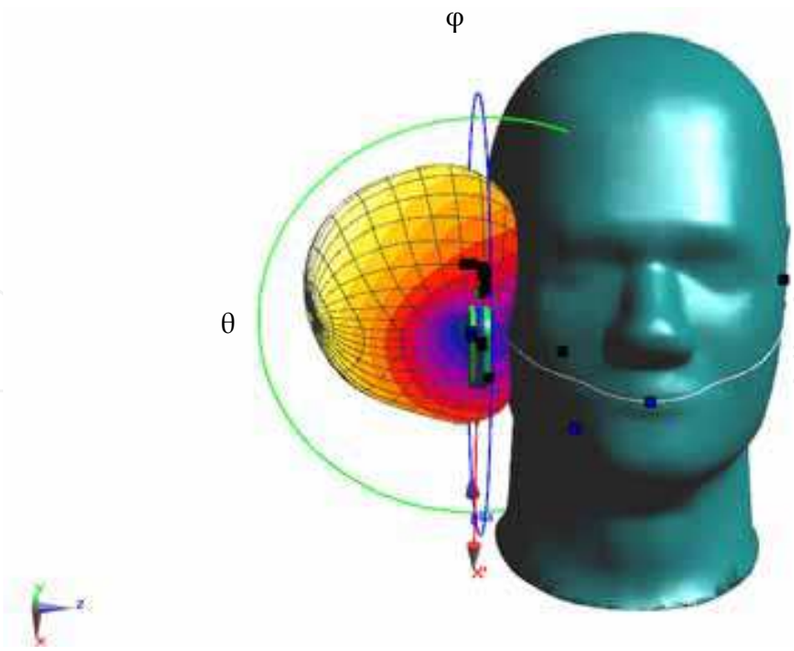

Fig. 17. Optimized 3D Far-field (θ , φ) radiation pattern image of the pilot radiator with Ni/Ag/Ni thin film internal antenna handset at 870MHz SAM condition (with SEMCAD program)

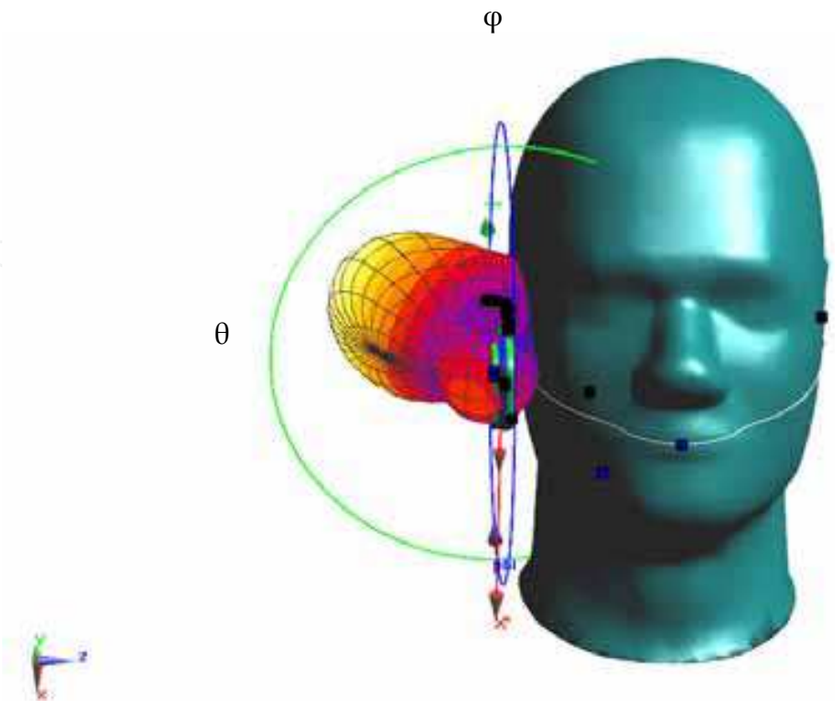

Fig. 18. Optimized 3D Far-field (θ , φ) radiation pattern image of the pilot radiator with Ni/Ag/Ni thin film internal antenna handset at 1990MHz SAM condition (with SEMCAD program)

3-D Far Field (θ , φ)	Free space		SAM	
	870MHz	1990MHz	870MHz	1990MHz
Total Radiated Power (P_{rad})	1.687W (32.27dBm)	0.853W (29.31dBm)	0.767W (28.84dBm)	0.676W (28.30dBm)
Total Isotropic Sensitivity (P_{TIS})	-105.28 dBm	-102.32dBm	-101.85dBm	-101.31dBm
Directivity (dB_i)	2.12	4.90	3.96	6.88
Gain (dB_i)	1.54	1.29	-0.17	2.20
Total Efficiency (η_{total})	0.84	0.42	0.38	0.34

Table 2. Comparisons of 3D Far-field (θ , φ) radiation pattern for the Ni/Ag/Ni sputter-deposit internal antenna handset at free space and SAM condition each frequencies (f = 870 MHz, 1990 MHz)

2.5 Characteristics of antenna performance with SAM condition

This section describes the radiation pattern characteristics of the carrier-based internal antenna and the sputter-deposit internal antenna. Figure 19 shows of radiation pattern results in SAM condition. The measured radiation pattern experiment is very significant for antenna performance aspects. At the same times this method can verify the close to real

human effect. Figure 19 shows of the measured data of peak and average gain for carrier-based internal antenna radiation patterns, Figure 19 (a) shows the E1-plane (y-z plane) measured result, Figure 19 (b) shows E2-plane (x-z plane) and Figure 19 (c) shows H-plane (x-y plane) characteristics at 869MHz and 1930MHz, the carrier-based internal antennas same to measured in an anechoic chamber complied with CTIA (CTIA Certification, 2005).

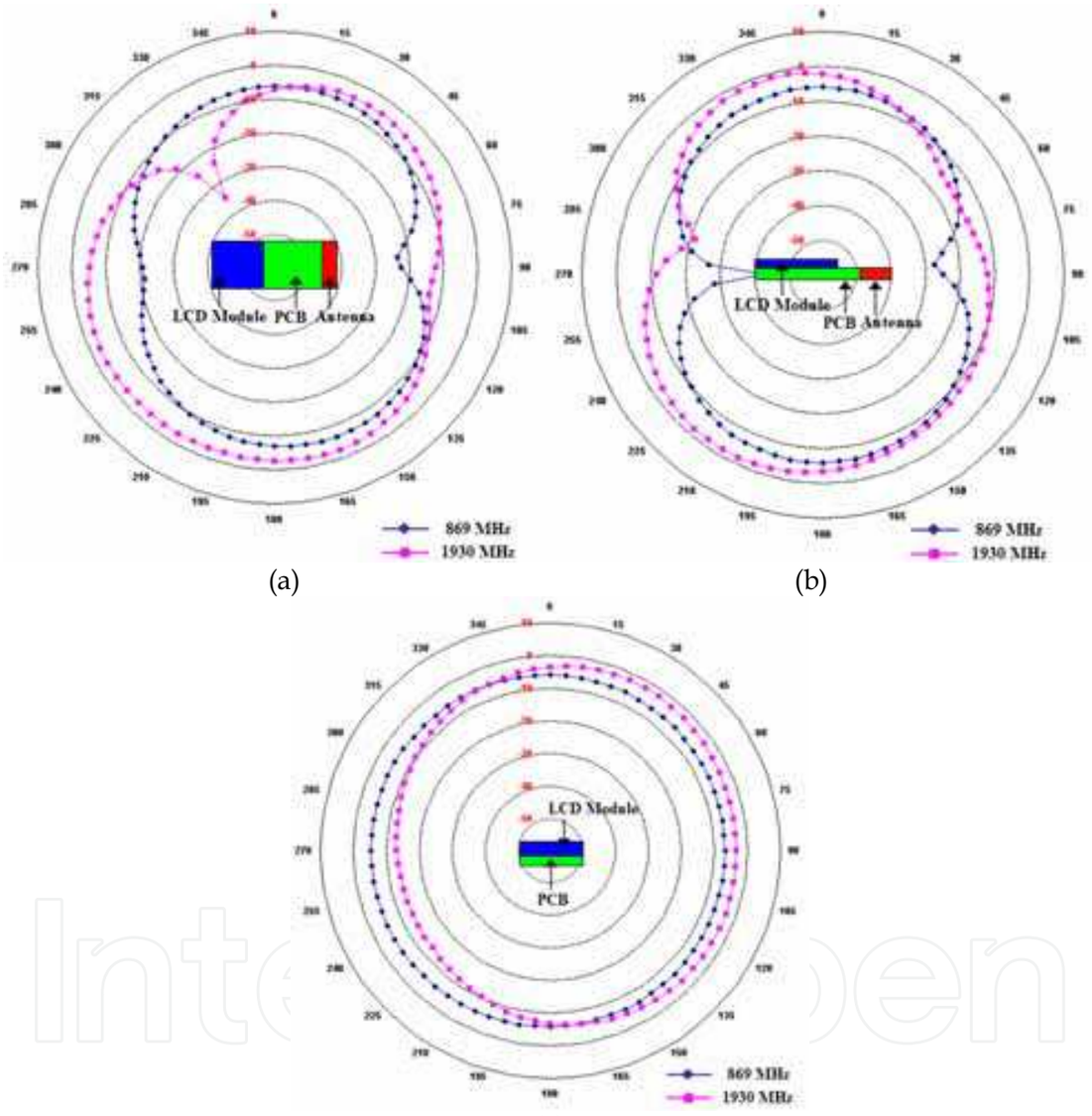

Fig. 19. Measured radiation pattern of E-plane and H-plane for the sputter-deposit Ni/Ag/Ni internal antenna handset at resonance (f = 869 MHz, 1930 MHz) (a) E1-plane, (b) E2-plane, (c) H-plane

The measured results of peak gain each E1, E2, and H-plane are listed in Table 3. Shows of the experiment result, the measured E1-plane (y-z) average radiation gains are each -6.05dBi and -5.55dBi at 869MHz and 1990MHz and then measured E2-planes (x-z) average radiation gains indicates -9.20dBi and -5.45dBi at 869MHz and 1930MHz also, the measured H-plane

(x-y) average radiation gains are each -9.20dBi and -5.34dBi at 869MHz and 1930MHz, respectively. Furthermore, measured E1-plane (y-z) peak radiation gain results are -5.92dBi (165 degree) and -2.49dBi (335 degree) at 869MHz and 1990MHz and then the measured E2-planes (x-z) peak radiation gains are -5.89dBi (355 degree) and -1.44dBi (345 degree) at 869MHz and 1930MHz also, the measured H-plane (x-y) peak radiation gains indicates -5.37dBi (250 degree) and -2.36dBi (30 degree) at 869MHz and 1930MHz, respectively.

Consequently, two kinds of internal antenna radiation pattern show good agreement as well as meet for CTIA regulation. Especially, the proposed Ni/Ag/Ni thin film internal antenna result shows come to good basis on experiment. Therefore, in this research is enormous benefit such as extended to antenna carrier volume and adapted diversity topology for next generation wireless mobile antenna solution also cost effective.

Frequency	E1-plane (y-z)	E2-plane (x-z)	H-plane (x-y)
Gain Average			
869 MHz	-6.05 dBi	-9.20 dBi	-5.97 dBi
1930 MHz	-5.55 dBi	-5.45 dBi	-5.34 dBi
Gain Peak			
869 MHz	-5.92 dBi, 5 deg	-5.89 dBi, 355 deg	-5.37 dBi, 250 deg
1930 MHz	-2.49 dBi, 165 deg	-1.44 dBi, 345 deg	-2.36 dBi, 30 deg
Gain min			
869 MHz	-23.61 dBi, 85 deg	-42.88 dBi, 270 deg	-6.87 dBi, 85 deg
1930 MHz	-35.00 dBi, 325 deg	-21.54 dBi, 285 deg	-13.70 dBi,245 deg

Table 3. Measured E-plane and H-plane radiation pattern for the Ni/Ag/Ni sputter-deposit PIFA antenna handset at resonance (f = 869 MHz, 1930 MHz), E1-plane (y-z plane), E2-plane (x-z plane), and H-plane (x-y plane)

2.6 Characteristics of field test

In this section, outlines evaluating for wireless handset performance through the analysis of voice quality and handset sensitivity measurements. In particular, this experiment is considered collected voice quality measurements in live-network test beds. This method is close to user experience. In this experiment discusses the collected voice quality measurement, handset sensitivity, and field trial performance. Figure 20 describes a sound source of speak British English and portion of speak British English with metrico field trial system. It means that measurements made using non-speech signals, such as tones or white noise, are unrepresentative and misleading. Metrico field experiments operate with 5 sec for each of two talkers (one male, one female), 10 sec in total (Metrico Muse system). Therefore, these sections discuss the field trial results between the carrier-based internal antenna handset and the proposed sputter-deposit internal antenna handset.

The experiments methods for data generation consist of the usage of mobile phones while make a call inside cars. On the contrary, communicated base station located in possible to make a connection. The metrico field trial system can verify the communication error and data generation interact with mobile phone, which is uplink and downlink paths. This experiment test bed is used on country lanes in Figure 21. To figure out how many times disconnect a call and the variation of electric field strength in worst GSM field area is the purpose of this experiment

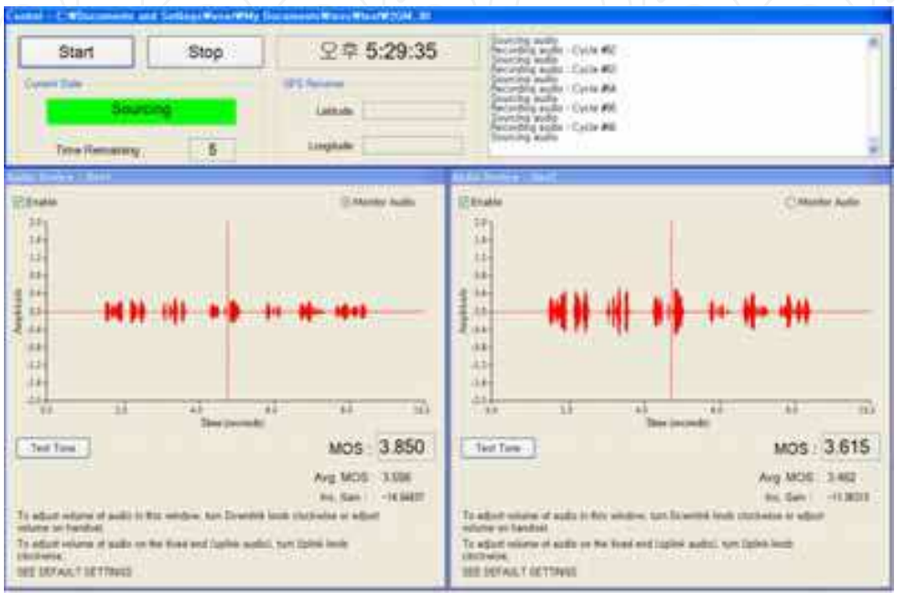

Fig. 20. Portion of the speak British English with metrico field trial system; 5 sec for each of two talkers (one male, one female), 10 sec in total

	Downlink MOS		**Uplink MOS**	
	Carrier-based Internal Antenna Handset	Sputter-deposit Internal Antenna Handset	Carrier-based Internal Antenna Handset	Sputter-deposit Internal Antenna Handset
Average	3.64	3.62	3.49	3.51
Standard Deviation	0.40	0.41	0.28	0.32
Maximum Score	4.10	4.07	3.92	3.94
Count	202	202	202	202
% MOS gather than 3.2	88%	87%	88%	85%
% MOS less than 3	9%	9%	7%	10%
% MOS less than 2.3	2%	1%	0%	1%

Table 4. Comparison of MOS distribution result the carrier-based internal antenna handset and the sputter-deposit based internal antenna handset at Maryland Baltimore Howard area (2G GSM network)

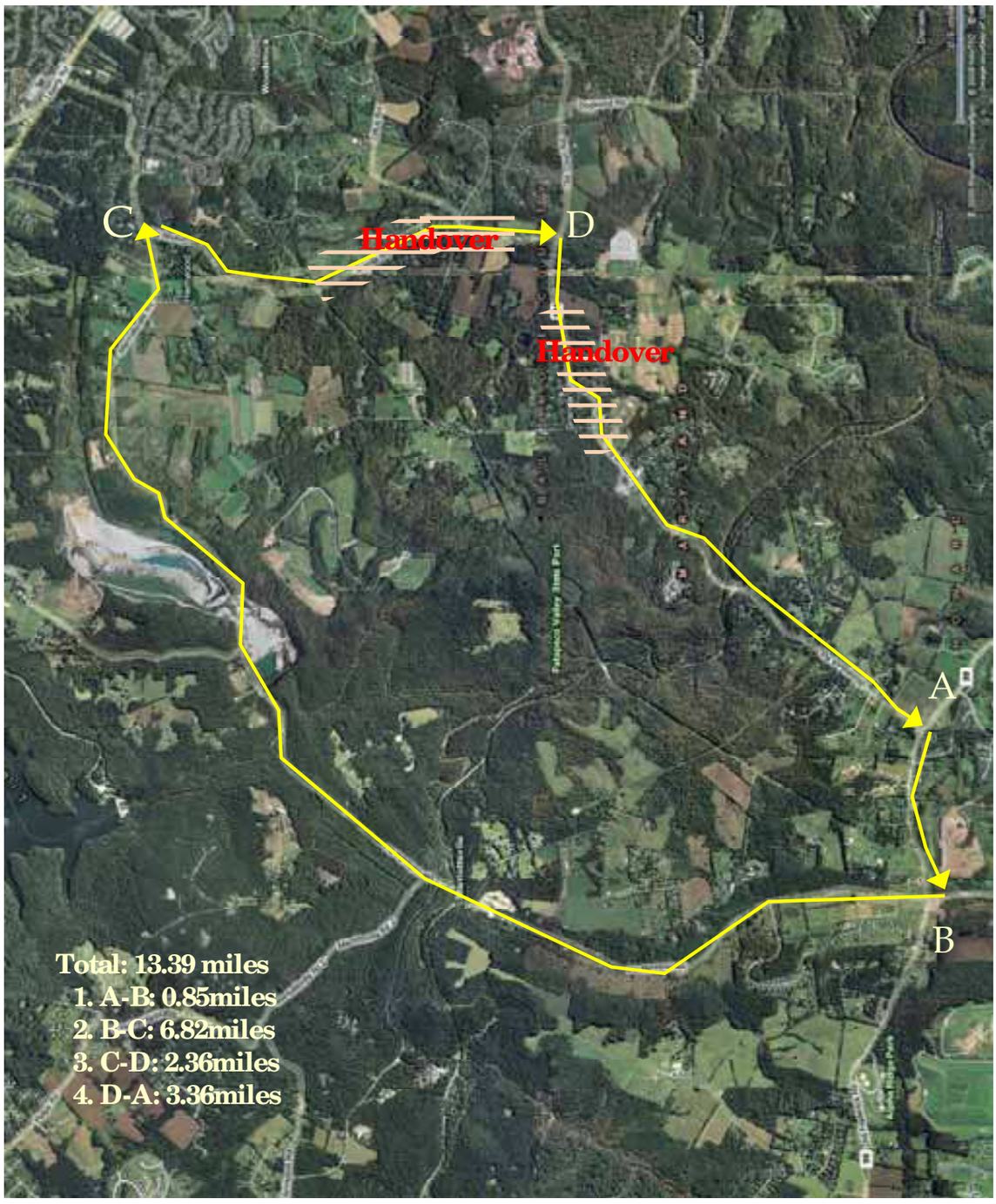

Fig. 21. Photo image of the 2G (GSM network) field trial route and the handover area information in USA (Microsoft Virtual Earth)

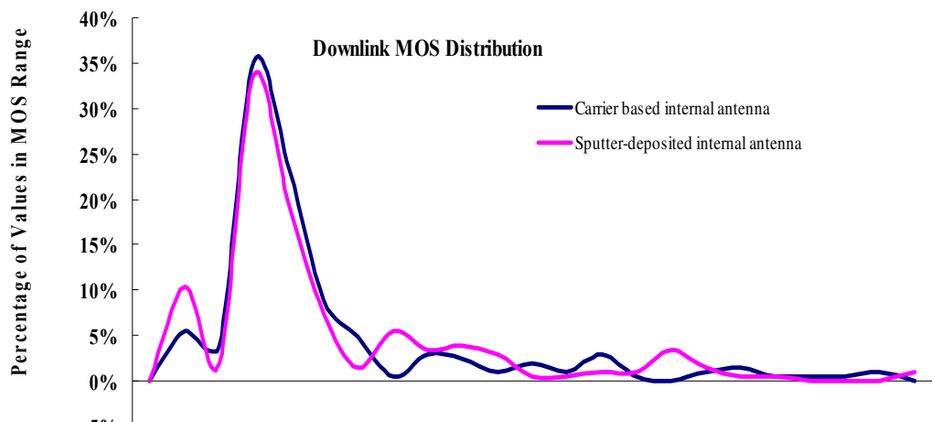

	>4.1	4.0-4.1	3.9-4.0	3.9-3.8	3.8-3.7	3.7-3.6	3.6-3.5	3.5-3.4	3.4-3.3	3.3-3.2	3.2-3.1	3.1-3.0	3.0-2.9	2.9-2.8	2.8-2.7	2.7-2.6	2.6-2.5	2.5-2.4	2.4-2.3	2.3-2.2	2.2-2.1	2.1-2.0	<2.0
Carrier based internal antenna	0%	5%	4%	35%	23%	9%	5%	0%	3%	2%	1%	2%	1%	3%	0%	0%	1%	1%	0%	0%	0%	1%	0%
Sputter-deposited internal antenna	0%	10%	2%	34%	19%	7%	1%	5%	3%	4%	3%	0%	0%	1%	1%	3%	1%	0%	0%	0%	0%	0%	1%

MOS Range

(a)

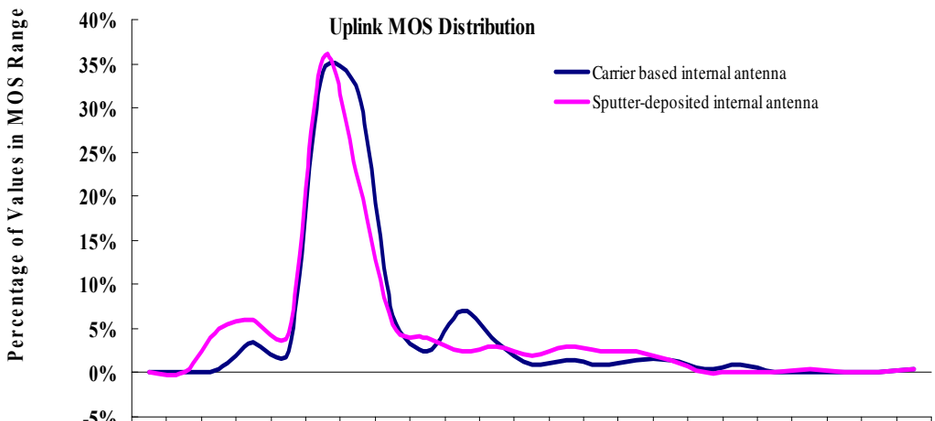

	>4.1	4.0-4.1	3.9-4.0	3.9-3.8	3.8-3.7	3.7-3.6	3.6-3.5	3.5-3.4	3.4-3.3	3.3-3.2	3.2-3.1	3.1-3.0	3.0-2.9	2.9-2.8	2.8-2.7	2.7-2.6	2.6-2.5	2.5-2.4	2.4-2.3	2.3-2.2	2.2-2.1	2.1-2.0	<2.0
Carrier based internal antenna	0%	0%	0%	3%	2%	34%	32%	6%	2%	7%	3%	1%	1%	1%	1%	1%	0%	1%	0%	0%	0%	0%	0%
Sputter-deposited internal antenna	0%	0%	5%	6%	4%	36%	22%	5%	4%	2%	3%	2%	3%	2%	2%	1%	0%	0%	0%	0%	0%	0%	0%

MOS Range

(b)

Fig. 22. Comparison of MOS distribution result the carrier-based internal antenna handset with sputter-deposit based internal antenna handset at Maryland Baltimore in USA (2G GSM network)

Figure 22 shows MOS distribution profile between the carrier-based internal antenna handset and the proposed sputter-deposit internal antenna handset in Maryland Baltimore Howard area. Computed the total distance is 13.39miles, Serving cell and neighbor cell network indicates each 133, 142, 145, 146 channel in GSM850 band also indicates 636, 630, 670 channel in GSM 1900 at start place, until now measured Rx sensitivity range is -80dBm to -103dBm around A boundary. Also bring about network handover at C to D area and D to A area in Figure 21. Figure 23 shows the real-log data about D to A handover area. Table 4 shows MOS distribution result comparison between the carrier-based internal antenna handset and the proposed sputter-deposit internal antenna handset. As a result, two kinds of handsets average MOS score marks over 3.0. Namely, carrier-based internal antenna handset and the sputter-deposit internal antenna handset is "fair" and "Good" performance in Uplink and Downlink paths. Because of Metrico field trial system basis on ITU defined theory, in other words, ITU defined voice quality ratio at five-point scale each called the mean opinion score (MOS) step, where 1 is poor and 5 is excellent quality. Therefore, the proposed sputter-deposit internal antenna handset shows good performance in the GSM network (ITU-T Rec., 2001).

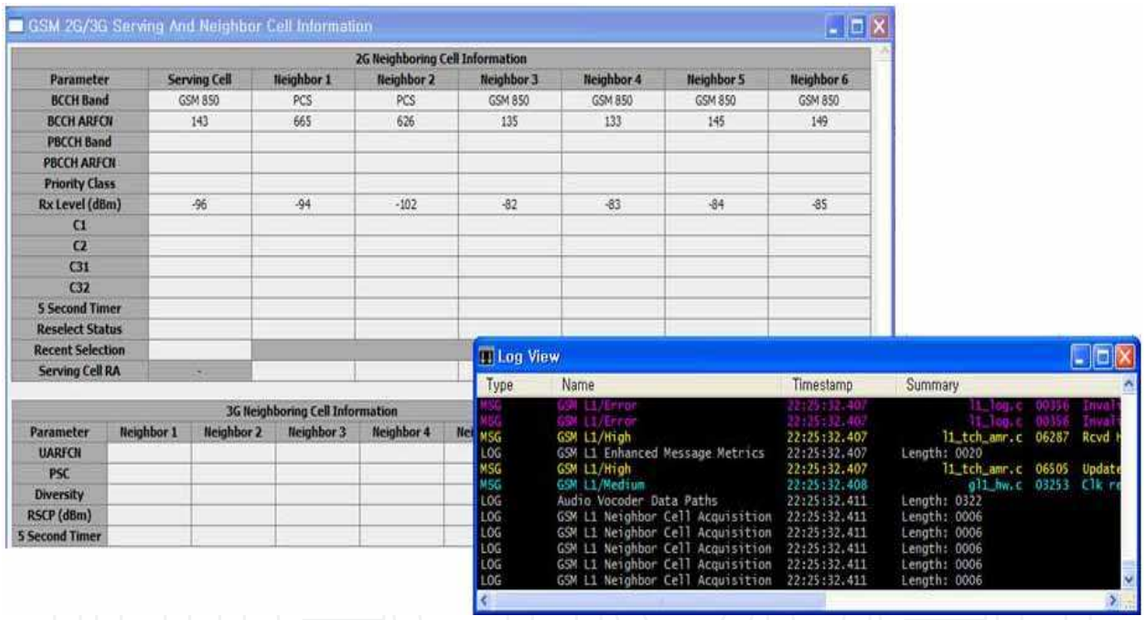

Fig. 23. Field trial log information of the GSM 2G network serving and Neighbor cell nearby Old Frederick Rd 99 and Woodstock Rd subway 125 junctions

3. Conclusion

This chapter fabricated and estimated of the novel Ni/Ag/Ni thin film internal antenna. Also, experiment characteristics of SWR and efficiency aspect for the proposed Ni/Ag/Ni thin film solution. The experiment Ni/Ag/Ni thin film internal antennas overall size is 43.0 × 24.0 × 0.0015mm^3 without feeding mechanism. As the demonstrated results, the proposed Ni/Ag/Ni thin film internal antenna has dual resonances in frequency which is suitable for a quad-band mobile communication system. Furthermore, the proposed Ni/Ag/Ni sputter-deposit planar inverted-F antenna occupies attractive size in volume. Briefly speaking of the

this experiment results, in this chapter reviewed fabrication process and characteristics for the Ni/Ag/Ni thin film internal antenna by sputter-deposited on polycarbonate substrate with 1.5um thickness, which is layers sputtered each 3,000Å, 8,000Å and 4,000Å, respectively. As a result, this solution is proven out last layer has characteristics of both materials Ag and Ni in distribution material spread spectrum. Moreover, the optimized SWRs and gain characteristics of radiation patterns are suitable for quad-band antenna. Also, this experiment verified comparison with carrier-based internal antenna having 40.4 × 19.2 × 6.25mm^3 volumes as well as this research performed current distribution and efficiency simulation used by CST and SEMCAD computing program.

The objective of this research is to perform an interaction with human head and field experiments used the carrier-based internal antenna and the sputter-deposit Ni/Ag/Ni thin film internal antenna. This research has the previous test result of radiation pattern characteristics with SAM condition from 824MHz to 1990MHz each E1, E2 and H plane on both side antennas. Also, this research is investigated for field trial effect comparing with reference handset including carrier-based internal antenna handset and the proposed sputter-deposit internal antenna handset having the Ni/Ag/Ni thin films at each 2G, 3G, and DOOC live-network test beds. As a consequence, the proposed sputter-deposit internal antenna handset obtained over 3.0 MOS score in the GSM network also, over 3.5 MOS score at WCDMA live-network at Baltimore Maryland in USA. The real field test result shows that the performance of the proposed Ni/Ag/Ni sputter-deposit internal antenna is almost same as carrier-based internal antenna, and especially at the 3G field, the strength of electric field is very stable. And then, this study found that the evidence converging to support the experiments from interaction with human head effect and field trial results (2G, 3G and DOOC field trial)

To conclude, this research is very attractive for adapting to wireless applications such as portable antenna, MediaFLO antenna, and so on. Furthermore, the Ni/Ag/Ni thin film internal antenna radiation performances show good agreement as well as meet for CTIA regulation and field test performances. Therefore, I firmly hold a view that the sputter-deposit internal antennas exercise is a far-reaching positive influence upon wireless mobile systems and embed modem or device application having several GHz for next generation mobile solution that is also cost effective.

4. References

F. Adachi, M. Sawahashi, and H. Suda, Wideband DS-CDMA for Next Generation Mobile Communications Systems, *IEEE Communications Magazine*, Vol. 36, pp. 56-69, 1998.

K. Hirasawa and M. Haneishi, Analysis, Design, and Measurement of Small and Low Profile Antennas, Artech House, ISBN 0-89006-486-5, 1991.

W. L. Stutzman and G. A. Thiele, Antenna Theory and Design, *John Willy & Sons Inc. press*, 1998.

D. Yuepeng, The Film Sputtering of Gadolinium and Chromium-doped Yttrium Aluminum Garnet, Ph.D Dissertation, *The University of Tennessee*, Knoxville, pp.1-14, 2005.

G. C. Stutzin, K. Rozsa, and A. Gallangher, Vacuum, Surface, and Films, *Journal of Vacuum* Science *& Technology*, Vol. 11, p 647, 1993.

CTIA Certification, Test Plan for Mobile Station over the Air Performance, Revision 2.1, *CTIA*, p.142, 2005.

C. T. P. Song, P. S. Hall, P. S. Ghafouri-Shiraz, and D. Wake, Triple Band Planar Inverted F Antennas for Handheld Devices, *Electronics Lett.*, Vol.36, p.112, 2000.

ITU-T Rec., An Objective Method for End-to-end Speech Quality Assessment of Narrowband Telephone Networks and Speech Codecs, *International Telecommunication Union*, Geneva, Switzland, P.862, 2001.

Metrico Muse system, http://www.metricowireless.com/

Microsoft Virtual Earth, http://maps.msn.com/

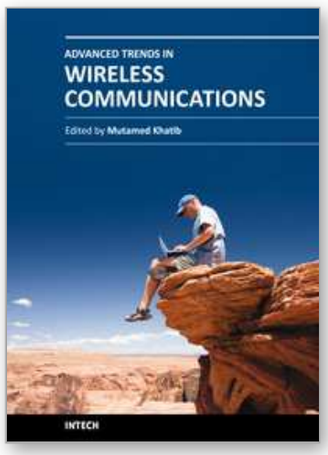

Advanced Trends in Wireless Communications

Edited by Dr. Mutamed Khatib

ISBN 978-953-307-183-1
Hard cover, 520 pages
Publisher InTech
Published online 17, February, 2011
Published in print edition February, 2011

Physical limitations on wireless communication channels impose huge challenges to reliable communication. Bandwidth limitations, propagation loss, noise and interference make the wireless channel a narrow pipe that does not readily accommodate rapid flow of data. Thus, researches aim to design systems that are suitable to operate in such channels, in order to have high performance quality of service. Also, the mobility of the communication systems requires further investigations to reduce the complexity and the power consumption of the receiver. This book aims to provide highlights of the current research in the field of wireless communications. The subjects discussed are very valuable to communication researchers rather than researchers in the wireless related areas. The book chapters cover a wide range of wireless communication topics.

How to reference

In order to correctly reference this scholarly work, feel free to copy and paste the following:

Book-Sung Park, Hyun-Sang Lee and Soren Pedersen (2011). Fabrication and Characterizations of Multi-Layer Thin Film Internal Antenna for Wireless Communication, Advanced Trends in Wireless Communications, Dr. Mutamed Khatib (Ed.), ISBN: 978-953-307-183-1, InTech, Available from: http://www.intechopen.com/books/advanced-trends-in-wireless-communications/fabrication-and-characterizations-of-multi-layer-thin-film-internal-antenna-for-wireless-communicati

INTECH
open science | open minds

InTech Europe
University Campus STeP Ri
Slavka Krautzeka 83/A
51000 Rijeka, Croatia
Phone: +385 (51) 770 447
Fax: +385 (51) 686 166
www.intechopen.com

InTech China
Unit 405, Office Block, Hotel Equatorial Shanghai
No.65, Yan An Road (West), Shanghai, 200040, China
中国上海市延安西路65号上海国际贵都大饭店办公楼405单元
Phone: +86-21-62489820
Fax: +86-21-62489821

IntechOpen